Sonoelastographic Shear Velocity Imaging: Experiments on Tissue Phantom and Prostate

K. Hoyt, K. J. Parker and D. J. Rubens
Rochester Center for Biomedical Ultrasound
University of Rochester, Rochester, NY 14627 USA

***Abstract*—In this paper, we introduce and evaluate a novel sonoelastographic technique for imaging shear velocity distributions from propagating shear wave interference patterns (termed crawling waves). A mathematical relationship between local crawling wave spatial phase derivates and shear velocity is presented with phase derivatives estimated using an autocorrelation-based technique. Results from homogeneous phantoms illustrate the ability of sonoelastographic shear velocity imaging to accurately quantify the true shear velocity distribution as verified using time-of-flight measurements. Results from a heterogeneous phantom reveal the ability of sonoelastographic shear velocity imaging to distinguish a stiff circular inclusion with shear velocity contrast comparable to that measured using mechanical testing techniques. High contrast visualization of focal carcinomas in an in-vitro prostrate specimen demonstrates the feasibility of this novel sonoelastographic imaging technique in tissue.**

Keywords-crawling waves; elasticity imaging; shear velocity estimation; sonoelastography.

I. INTRODUCTION

Ultrasound-based methods for imaging the elastic properties of soft tissue have become a diverse international research endeavor [1-3]. In general, the universal goal of these efforts is to map some tissue mechanical property in an anatomically meaningful manner to provide useful clinical information. Since changes in tissue stiffness are typically symptomatic of an abnormal pathological process, tissue elasticity imaging is a relatively new and promising modality for differentiating normal from abnormal tissues.

Vibrational (or dynamic) sonoelastography is an elasticity imaging technique that estimates the amplitude response of tissue under forced harmonic excitation using ultrasonic Doppler techniques [4]. Due to a mathematical relationship between particle vibrational response and the received Doppler spectral variance [5], the amplitude of propagating shear waves in tissue can be visualized in real-time using sonoelastography (images are termed sonoelastograms) to identify regions of abnormal stiffness [6].

Recently, it was shown that interfering shear waves could produce slowly propagating interference patterns with an apparent velocity much less than (but proportional to) the underlying true shear velocity [7]. Termed crawling waves, they can be produced using a pair of mechanical sources vibrating at slightly offset frequencies and visualized in real-time using sonoelastographic imaging. Since crawling waves describe shear wave propagation patterns, the resultant image information can be analyzed to estimate spatial elastic properties such as shear velocity distributions [8].

II. THEORY

A. Shear Wave Interference Patterns

Consider two equal amplitude shear wave excitation sources positioned laterally (separation distance D) on opposite sides of a medium. If the sources vibrate at frequencies ω_S and $\omega_S + \Delta\omega_S$, respectively, then the propagating shear waves can be expressed as

$$u_1(x,t) = A\exp\left[-\alpha\left(x+\frac{D}{2}\right)\right]\exp\left[ik_S\left(x+\frac{D}{2}\right)+i\omega_S t\right] \quad (1)$$

$$u_2(x,t) = A\exp\left[-\alpha\left(\frac{D}{2}-x\right)\right]\exp\left[\begin{matrix} i(k_S+\Delta k_S)\left(\frac{D}{2}-x\right) \\ +i(\omega_S+\Delta\omega_S)t \end{matrix}\right] \quad (2)$$

where u_1 and u_2 are the instantaneous right and left propagating waves, respectively, A is the source amplitude, α is the shear wave attenuation coefficient, k_S and Δk_S are the shear wave number and difference, respectively [7]. If the shear wave sources are relatively far away compared to the field of view, then the waves from each source can be considered plane waves [7]. Thus, the shear wave interference pattern U is the superposition of eqns (1) and (2) and can be written as

$$U(x,y,t) = u_1(x,t) + u_2(x,t). \quad (3)$$

indicating that for a homogeneous medium the crawling wave patterns are a set of harmonic signals independent of vertical position.

Since sonoelastography estimates the magnitude of a vibrating target, an alternative form of eqn (3) is required to recover a mathematical expression for a harmonic signal, or more specifically

$$\left|U(x,y,t)\right|^2 = \left[u_1(x,t)+u_2(x,t)\right]*\left[u_1^*(x,t)+u_2^*(x,t)\right] \quad (4)$$

where u^* is the complex conjugate of u. Combining eqns (1), (2) and (4) yields the following expression

$$|U(x,y,t)|^2 = 2A^2 \exp(-\alpha D)\times \left[\cosh(2\alpha x)+\cos(2k_S x+\Delta k_S x+\Delta\omega_S t)\right] \quad (5)$$

Finally, sampling of the crawling wave displacement field described by eqn (5) results in

$$s(m,n,r) = 2A^2 \exp(-\alpha D)\times \left[\cosh(2\alpha n T_n)+\cos(2k_S n T_n+\Delta k_S n T_n+\Delta\omega_S r T_r)\right] \quad (6)$$

where m, n, and r are integer values, and T_n and T_r are the spatial and temporal sampling intervals, respectively.

B. Shear Velocity Estimation

In regards to eqn (6), the shear velocity can be found by taking the spatial derivative of the phase argument along the shear wave propagation axis as

$$\frac{\partial\phi}{\partial n} = \frac{\partial(2k_S n T_n+\Delta k_S n T_n)}{\partial n} = (2k_S+\Delta k_S)T_n \quad (7)$$

By introducing the following expressions: $k_S = 2\pi f_S/c_S$ and $\Delta k_S = 2\pi\Delta f_S/c_S$, where $f_S = \omega_S/2\pi$ and $\Delta f_S = \Delta\omega_S/2\pi$, then eqn (7) can be written as a function of the shear velocity c_S as

$$\frac{\partial\phi}{\partial n} = \frac{2\pi(2f_S+\Delta f_S)T_n}{c_S}. \quad (8)$$

However, since only discrete spatial data are available, only an approximation to the derivative in eqn (8) can be computed in practice. One computationally efficient method for doing such is the autocorrelation-based technique [9], which requires complex valued data sequences. If we consider the discrete-time shear wave displacement field described by eqn (6), the analytic signal s_A can be calculated efficiently using fast Fourier transform techniques [10]. Therefore, using a kernel window size of N samples, the first lag of the autocorrelation function $\hat{R}$ can be approximated as

$$\hat{R}(1) = \frac{1}{N-1}\sum_{z=1}^{N-1} s_A^*(z)s_A(z+1) \quad (9)$$

where data is taken parallel to the crawling wave propagation axis. Given the discrete autocorrelation estimates of eqn (9), the phase derivative is

$$\frac{\partial\phi}{\partial n} = \tan^{-1}\left[\frac{\Im\{\hat{R}(1)\}}{\Re\{\hat{R}(1)\}}\right]. \quad (10)$$

where $\Im\{\bullet\}$ and $\Re\{\bullet\}$ denote the imaginary and real parts, respectively [9]. Combining eqns (10) and (8) and rearranging the terms produces the expression

$$c_S = \frac{2\pi(2f_S+\Delta f_S)T_n}{\tan^{-1}\left[\frac{\Im\{\hat{R}(1)\}}{\Re\{\hat{R}(1)\}}\right]} \quad (10)$$

which indicates that the shear velocity can be estimated from the crawling wave spatial patterns given *a priori* knowledge of the source vibration frequencies and spatial sampling rate. By translating a kernel window across the image plane in the direction of shear wave propagation and repeating for each depth location, local shear velocity estimates can be obtained for each spatial position using eqn (10). The resultant data field is imaged and describes the 2D spatial shear velocity distribution.

III. Materials and Methods

Two bending piezoelectric elements termed biomorphs (Piezo Systems, Cambridge, MA USA) functioned as the vibration sources. A dual channel signal generator (Model AFG320, Tektronix, Beaverton, OR USA) produced two slightly offset monochrome signals that were passed through a two channel power amplifier before being input to the biomorphs. A LOGIQ 9 scanner (General Electric Medical Systems, Milwaukee, WS USA) modified for sonoelastography was used with a M12L linear array probe (5–13 MHz bandwidth) for real-time visualization of propagating crawling waves (scan plane orthogonal to shear wave propagation axis). Demodulated IQ data sets were stored and transferred to an external computer for processing.

Regarding the first set of validating experiments, we evaluated two homogeneous gelatin phantoms of differing stiffness. Shear velocities were measured using time-of-flight methods [7] for comparison to shear velocity imaging results. In the second experiment, a heterogeneous phantom containing a 1 cm stiff circular inclusion was used for preliminary assessment of shear velocity image contrast. Mechanical measurements were performed on both background and inclusion samples to obtain the respective elastic properties [11]. Lastly, shear velocity images were obtained from an excised prostate gland obtained immediately following radical prostatectomy. The excised gland was embedded in agar [12] and imaged using the same protocol as described for the phantom studies. The final diagnosis was obtained from the surgical pathology report. Note that tissue specimen use was IRB approved and HIPAA compliant. Informed consent was obtained for use of the excised gland.

For all experimental results, shear wave attenuation effects were minimized by suppressing the first two Fourier series coefficients when computing the analytic image sets and prior to shear velocity estimation. This approach is analogous to highpass filtering and is implemented in a computationally efficient manner.

IV. Results

The results of Fig. 1 illustrate the crawling wave sonoelastograms (i.e., shear wave interference patterns) and matching shear velocity images from the two homogeneous phantoms. For a given vibration frequency, the spatial

frequency of the harder phantom is lower compared to the softer phantom, indicating an increase in the true shear velocity distribution. For the shear velocity sonoelastograms, an increase in phantom stiffness corresponds to an increase in shear velocity estimates and is independent of vibration frequency, although at higher vibration frequencies, the shear velocity sonoelastograms exhibit artifacts that are attributed to increased attenuation effects that were not compensated for using amplitude normalization. Statistical results were obtained from these phantoms and compared to measured shear velocities shown in Fig. 2. As these results indicate, the shear velocity sonoelastograms closely match the true distribution in the range of vibration frequencies investigated.

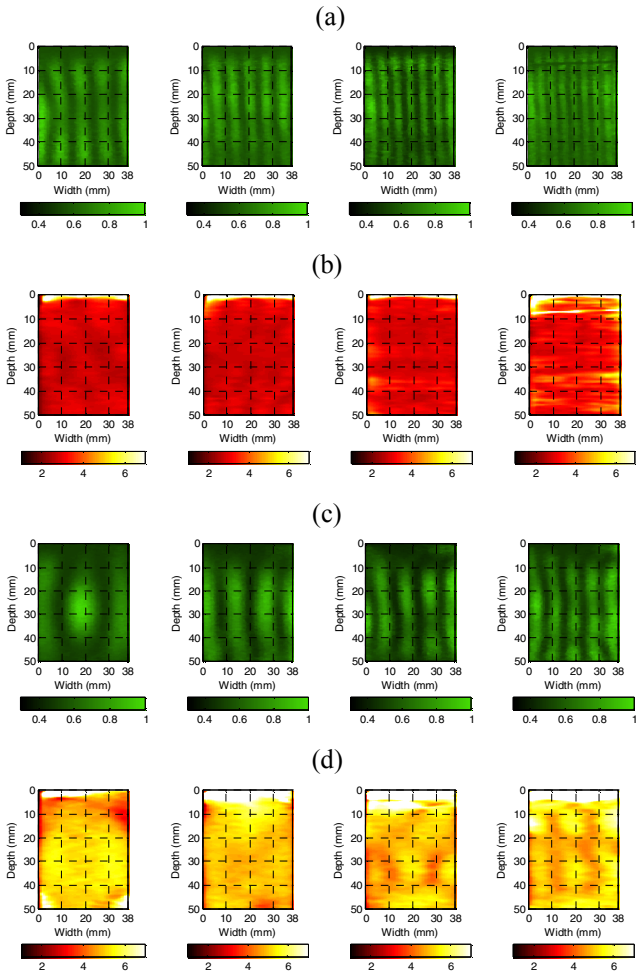

Figure 1. Crawling wave sonoelastograms from homogeneous phantoms of relatively (a) low and (c) high stiffness (using shear wave vibration frequencies of 150, 200, 250 and 300 Hz, left to right, respectively and Δf of 0.15 Hz). Matched shear velocity images (averaged over 20 images) are also shown in (b) and (d), respectively.

Results from the heterogeneous phantom are illustrated in Fig. 3. Although not apparent from the crawling wave patterns, the shear velocity sonoelastogram depicts a high contrast inclusion. Mechanical measurements from material samples revealed a shear velocity contrast of 1.48 compared to a contrast of 1.5 as derived from the imaging results.

Shear velocity imaging results from the in-vitro prostate specimen are presented in Fig. 4. Notice that the shear velocity sonoelastogram indicates two distinct regions in the left and right gland of elevated shear velocity that are not visualized on the B-mode ultrasound image. The pathology report confirmed these two regions as focal carcinomas.

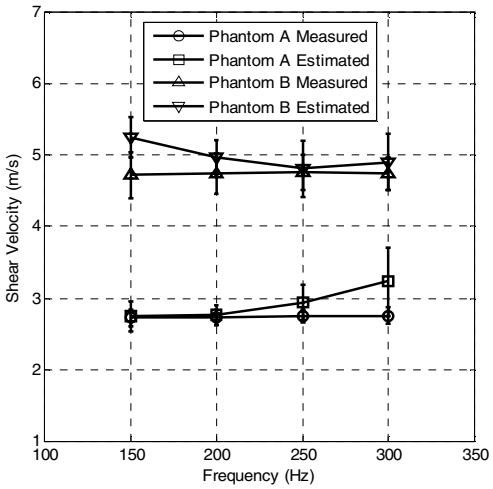

Figure 2. Matched shear velocity estimates from shear velocity sonoelastogram stacks and physical measurements (i.e., time-of-flight). Statistics were computed as a function of vibration frequency and from the relatively soft (Phantom A) and hard (Phantom B) homogeneous phantoms.

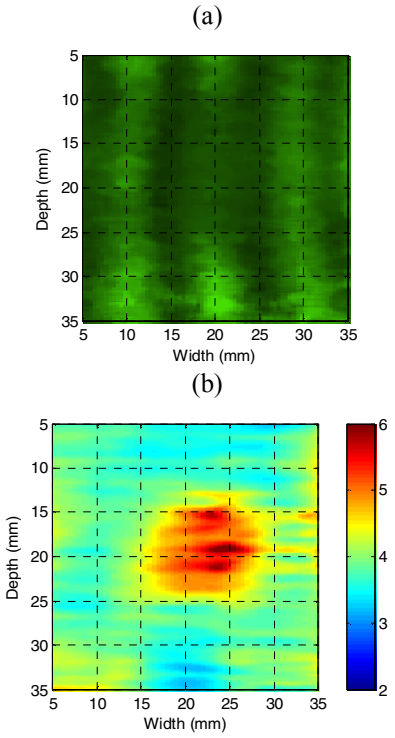

Figure 3. (a) Crawling wave and (b) shear velocity sonoelastograms (averaged over 20 images) from heterogeneous phantom (1 cm diameter stiff inclusion). Results were obtained using vibration frequencies of 200 and 200.15 Hz.

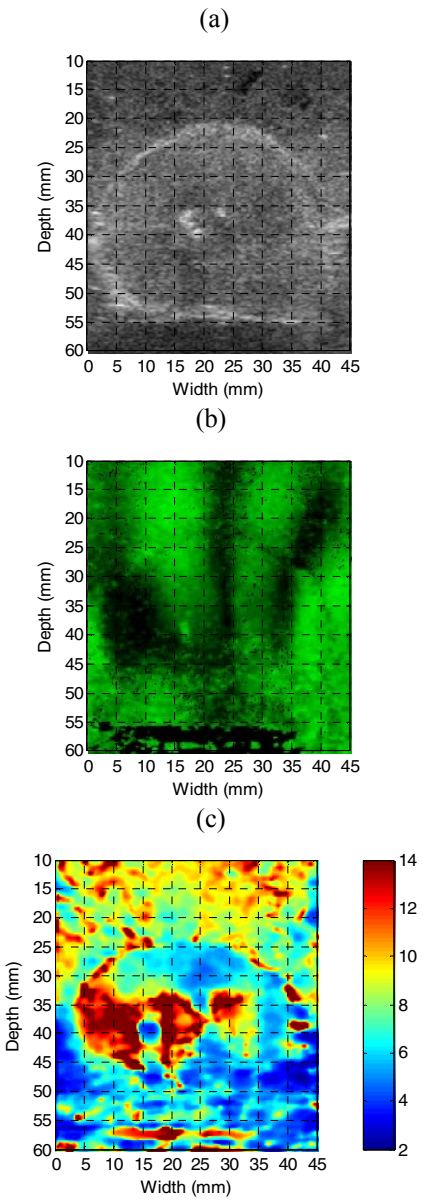

Figure 4. Results from in-vitro prostate gland experiments. Results depict the matched (a) B-mode ultrasound image, (b) crawling wave sonoelastogram and (c) shear velocity sonoelastogram (averaged over 20 images). Notice that the shear velocity sonoelastogram depicts two distinct regions of elevated shear velocities confirmed as focal carcinomas by pathological assessment and not evident in the B-mode ultrasound image.

V. CONCLUSIONS

In this paper, we introduced a novel sonoelastographic technique for estimating local shear velocities from crawling wave sonoelastograms. Results from homogeneous phantoms demonstrated the ability of sonoelastographic shear velocity imaging to quantify the true underlying shear velocity distributions as verified using time-of-flight measurements. Furthermore, heterogeneous phantom results revealed the ability to detect lesions (1 cm diameter inclusion) and quantify the shear velocity as validated from mechanical measurements on phantom samples. Experimental results from an in-vitro prostate specimen demonstrated feasibility for sonoelastographic shear velocity imaging in tissue.

ACKNOWLEDGMENT

The authors thank Dr. Zhe Wu of General Electric (GE) Medical Systems and Benjamin Castaneda and Man Zhang of the University of Rochester for their helpful suggestions. We also thank GE for their expertise and the loan of equipment. This research is supported by NIH Grant 5 R01 AG016317-05.

REFERENCES

[1] L. Gao, K.J. Parker, R.M. Lerner, and S.F. Levinson, "Imaging of the elastic properties of tissue – A review," Ultrasound Med. Biol., vol. 22, pp. 959-977, 1996.

[2] J. Ophir, S.K. Alam, B. Garra, F. Kallel, E. Konofagou, T. Krouskop and T. Varghese, "Elastography: Ultrasonic estimation and imaging of the elastic properties of tissues," Proc. Instn. Mech. Engrs., vol. 213, pp. 203-233, 1999.

[3] J. Greenleaf, M. Fatemi, and M. Insana, "Selected methods for imaging elastic properties of biological tissues," Annu. Rev. Biomed. Eng., vol. 5, pp. 57-78, 2003.

[4] R.M. Lerner, K.J. Parker, J. Holen, R. Gramiak and R.C. Waag, "Sonoelasticity: Medical elasticity images derived from ultrasound signals in mechanically vibrated targets," Acoust. Imaging, vol. 16, pp. 317-327, 1988.

[5] S.R. Huang, R.M. Lerner and K.J. Parker, "On estimating the amplitude of harmonic vibration from the Doppler spectrum of reflected signals," J. Acoust. Soc. Am., vol. 88, pp. 310-317, 1990.

[6] K.J. Parker, D. Fu, S.M. Gracewski, F. Yeung and S.F. Levinson, "Vibration sonoelastography and the detectibility of lesions," Ultrasound Med. Biol., vol. 24, pp. 1937-1947, 1998.

[7] Z. Wu, L.S. Taylor, D.J. Rubens and K.J. Parker, "Sonoelastographic imaging of interference patterns for estimation of the shear velocity of homogeneous biomaterials," Phys. Med. Biol., vol. 49, pp. 911-922, 2004.

[8] Z. Wu, K. Hoyt, D.J. Rubens and .K.J. Parker, "Sonoelastographic imaging of interference patterns for estimation of shear velocity distributions in biomaterials," J. Acoust. Soc. Am., vol. 120, pp. 535-545, 2006.

[9] C. Kasai, K. Namekawa, A. Koyano and R. Omoto, "Real-time two-dimensional blood flow imaging using an autocorrelation technique," IEEE Trans. Sonics Ultrason., vol. 32, pp. 458-464, 1985.

[10] S.L. Marples, "Computing the discrete-time analytic signal via FFT," IEEE Trans. Signal Processing, vol. 47, pp. 2600-2603, 1999.

[11] L.S. Taylor, M.S. Richards, A.J. Moskowitz, A.L. Lerner, D.J. Rubens and K.J. Parker, "Viscoelastic effects in sonoelastography: Impact on tumor detectibility," IEEE Ultrason. Sympos., pp. 1639-1642, 2001.

[12] L.S. Taylor, D.J. Rubens, B.C. Porter, Z. Wu, R.B. Baggs, P.A. di Sant'Agnese, G. Nadasdy, D. Pasternack, E.M. Messing, P. Nigwekar and K.J. Parker, "Prostate cancer: Three dimensional sonoelastography for in vitro detection," Radiology, vol. 237, pp. 981-985, 2005.